bandpass-filtered to remove the slowly varying background intensity produced by the support and shows how some of the atom features are distinctly more intense than the majority. The column intensity distribution is predominantly bimodal, with the more intense features having a mean intensity 2.5 times that of the majority. The intensity of the disordered single atoms visible at the top of the raft in Fig. 3C calibrates the intensity distribution. The more intense features are then consistent with two atoms arranged vertically in a column, because the resultant partially coherent scattering raises the intensity ratio above 2.

It is at first sight surprising that the isolated feature in the lower right of Fig. 3C and some of the atom sites at the edge of the raft should contain two atoms in a column. The absence of neighboring single-height columns raises the question of how these features are supported on the surface. A possible explanation is that some Rh atoms have been absorbed into the first layer of the alumina lattice, which would then allow the possibility of isolated pairs of Rh atoms arranged in a single column. Indeed, Yao *et al.* (*13*) have suggested dissolution of Rh into γ-Al_2O_3 as a degradation mechanism, a view that is supported by these observations.

Recently, first-principle calculations have been successfully applied to catalytic systems (*14*). It should now be possible, using the information from high-resolution Z-contrast microscopy, to calculate the electronic structure of the observed metal cluster configurations and relate it to the catalytic activity experimentally observed. Researchers could also study directly the mechanisms of catalyst degradation by imaging a series of specimens. We believe that the information about the metal support configuration now available in the microscope will facilitate a more detailed understanding of catalyst activity and degradation mechanisms.

REFERENCES AND NOTES

1. For example, L. Spenadel and M. Boudart, *J. Phys. Chem.* **64**, 204 (1960); S. F. Adler and J. J. Keavney, *ibid.*, p. 208.
2. Reviewed by D. C. Koningsberger and B. C. Gates [*Catal. Lett.* **14**, 271 (1992)].
3. For example, A. S. Fung, P. A. Tooley, M. J. Kelley, D. C. Koningsberger, B. C. Gates, *J. Phys. Chem.* **95**, 225 (1991).
4. D. E. Jesson and S. J. Pennycook, *Proc. R. Soc. London Ser. A* **449**, 273 (1995).
5. A. V. Crewe, J. Wall, J. Langmore, *Science* **168**, 1338 (1970).
6. M. S. Isaacson, D. Kopf, M. Ohtsuki, M. Utlaut, *Ultramicroscopy* **4**, 101 (1979).
7. M. S. Isaacson, M. Ohtsuki, M. Utlaut, in *Introduction to Analytical Electron Microscopy*, J. J. Hren, J. Goldstein, D. C. Joy, Eds. (Plenum, New York, 1979), pp. 343–368.
8. S. Iijima, *Optik* **48**, 193 (1977); A. K. Datye and D. J. Smith, *Catal. Rev. Sci. Eng.* **34**, 129 (1992).
9. M. M. J. Treacy and S. B. Rice, *J. Microsc.* **156**, 211 (1989).
10. J. M. Cowley, *Appl. Phys. Lett.* **15**, 58 (1969); E. Zeitler and M. G. R. Thomson, *Optik* **31**, 258 (1970).
11. A. J. McGibbon, S. J. Pennycook, D. E. Jesson, *J. Microsc.*, in press.
12. D. C. Koningsberger and M. Vaarkamp, *Physica B* **208-209**, 633 (1995).
13. H. C. Yao, S. Japar, M. Shelef, *J. Catal.* **50**, 407 (1977).
14. R. Shah, M. C. Payne, M.-H. Lee, J. D. Gale, *Science* **271**, 1395 (1996).

15. We thank D. R. Liu and E. Lowenthal for the provision of the catalyst samples. This work was performed at Oak Ridge National Laboratory, which is managed by Lockheed Martin Energy Research for the U.S. Department of Energy under contract DE-AC05-96OR22464, through an appointment to the Oak Ridge National Laboratory Postdoctoral Program administered by the Oak Ridge Institute for Science and Education.

28 May 1996; accepted 13 August 1996

Crystal Structure of DNA Recombination Protein RuvA and a Model for Its Binding to the Holliday Junction

John B. Rafferty, Svetlana E. Sedelnikova, David Hargreaves, Peter J. Artymiuk, Patrick J. Baker, Gary J. Sharples, Akeel A. Mahdi, Robert G. Lloyd, David W. Rice*

The *Escherichia coli* DNA binding protein RuvA acts in concert with the helicase RuvB to drive branch migration of Holliday intermediates during recombination and DNA repair. The atomic structure of RuvA was determined at a resolution of 1.9 angstroms. Four monomers of RuvA are related by fourfold symmetry in a manner reminiscent of a four-petaled flower. The four DNA duplex arms of a Holliday junction can be modeled in a square planar configuration and docked into grooves on the concave surface of the protein around a central pin that may facilitate strand separation during the migration reaction. The model presented reveals how a RuvAB-junction complex may also accommodate the resolvase RuvC.

Recombination is a potent evolutionary force that shapes and reshapes the genomes of all organisms. More than 30 years ago, Holliday (*1*) proposed a model of meiotic recombination in which homologous chromatids exchange single DNA strands to form a partially heteroduplex joint molecule with a four-way junction at the point of exchange (Fig. 1A). Resolution of the Holliday junction by symmetrical strand cleavage, coupled with repair of any DNA base pair mismatches in the heteroduplex regions, provided a plausible explanation for the formation of recombinants and for the patterns of marker segregation in genetic crosses. Although many features of the model have since been found wanting, the idea that recombinant chromosomes arise through the formation and subsequent resolution of Holliday intermediates has withstood the test of time (*2*). The reaction pathway has been dissected in detail in *Escherichia coli* (*3*). Eukaryotic homologs and analogs of the *E. coli* proteins are emerging (*4–6*), which leads to the expectation that the key features of the reaction mechanism will be generally, if not universally, applicable.

In the *E. coli* pathway, RecA protein polymerizes on single-strand tails at DNA ends or at single-strand gaps to form a helical nucleoprotein filament that promotes pairing and strand exchange with a homologous duplex (*7*). Strand exchange into regions of duplex-duplex pairing creates a Holliday intermediate that is then processed into mature products by RuvA, RuvB, and RuvC (*8*). RuvA and RuvB act in concert to provide a junction-specific DNA helicase that catalyzes branch migration (*9–12*). RuvA binds to the junction point (*9*, *10*) where it targets the assembly of RuvB, a hexameric ring helicase that provides the motor to drive the reaction (*13*). Electron micrographs of the tripartite complex reveal RuvA sandwiched between two diametrically opposed RuvB rings (*14*). Parsons *et al.* (*14*) suggested that the junction is held in a square-planar configuration with the two RuvB rings assembled around homologous arms and facing each other (Fig. 1B). Rotation of the duplex DNA by RuvB provides a simple model of how

J. B. Rafferty, S. E. Sedelnikova, D. Hargreaves, P. J. Artymiuk, P. J. Baker, D. W. Rice, Krebs Institute, Department of Molecular Biology and Biotechnology, University of Sheffield, Western Bank, Sheffield S10 2TN, UK.
G. J. Sharples, A. A. Mahdi, R. G. Lloyd, Department of Genetics, University of Nottingham, Queen's Medical Centre, Nottingham, NG7 2UH, UK.

*To whom correspondence should be addressed. E-mail: d.rice@sheffield.ac.uk

RuvAB could unwind and rewind strands to move the junction point along.

RuvC resolves Holliday intermediates into recombinant products (*15*, *16*). A dimer of RuvC binds the junction and makes symmetrically related incisions in strands of the same polarity (Fig. 1B) (*17*). The junction is in an unfolded configuration (*18*), in contrast to the stacked-X arrangement observed for synthetic junctions in the presence of cations but not complexed by protein (*19*). Cleavage occurs preferentially at a sequence with the consensus 5′-(A/T)TT ↓ (G/C)-3′ (where the arrow indicates the scissile bond) (*20*) and can occur in either of two orientations as predicted by the Holliday model (*16*, *18*, *21*). Whether RuvC targets naked-junction DNA or a RuvAB-junction complex remains unclear, although analysis of alternative resolution systems catalyzed by RecG helicase and RusA resolvase showed that RuvC cannot function in vivo without RuvAB (*22*–*24*).

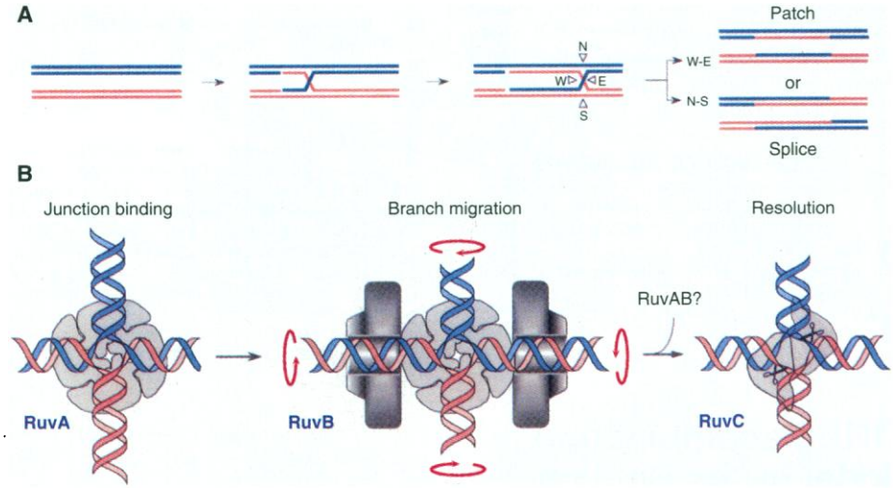

Fig. 1. The formation and resolution of a Holliday junction in homologous recombination in *E. coli*. (**A**) Schematic of the rearrangement undergone by DNA during homologous recombination. The parent duplexes are blue and pink, and the pairs of RuvC cleavage sites are marked N and S and W and E. (**B**) Arrangement of the protein and DNA components during the three stages of recombination catalyzed by the RuvABC system as proposed in the text and comparable with figure 4 in (*14*). The proteins are shown in overall outline. The two RuvB hexameric rings are presented in cross section with the DNA passing through their centers. The RuvC active sites are marked with the scissors symbols. The DNA is colored as in (A) and shown as double-stranded helices.

Crystals of RuvA belong to space group *P*4 with a monomer in the asymmetric unit (*25*), consistent with the known tetrameric quaternary structure of the protein in vitro (*26*, *27*). The structure was determined at a resolution of 1.9 Å by multiple isomorphous replacement (MIR) and anomalous scattering [(*28*) and Table 1]. A single-site mercury derivative was obtained through the covalent modification of Cys^{34} and a second derivative by incorporation of selenomethionine into the protein through growth of a RuvA-overexpressing strain (*29*) in a medium supplemented with selenomethionine. The latter gave a six-site derivative for which the difference Patterson function was solved by a genetic algorithm search procedure (*30*).

The final model of RuvA comprised 190 of the total 203 residues, with no interpretable density for a flexible loop between residues 143 and 155, inclusive. All side chains were fitted to the final model except those of residues His^{136}, Asp^{157}, Asp^{158}, Gln^{160}, Gln^{161}, Glu^{162}, Gln^{175}, Arg^{179}, Lys^{183}, Glu^{197}, Arg^{200}, and those in the flexible linker. A total of 54 solvent molecules were added in the later stages of refinement with a corresponding fall in the value of R_{free} of 2.7%. The crystallographic *R* factor is 20.9% for all data (17,090 reflections) in the resolution range of 15 to 1.9 Å. The model has good stereochemistry with values for the root-mean-square deviation from standard values of the bond lengths and angles of 0.016 Å and 1.9°, respectively. Representative parts of the electron density map are shown (Fig. 2, A and B); a Ramachandran plot of the model shows all nonglycine residues to be inside

Table 1. Data collection and phasing statistics. Crystals of RuvA were grown by the hanging-drop vapor-diffusion method from buffered NaCl solutions (*25*). The protein crystallizes in space group *P*4 with cell dimensions $a = b = 83.7$ Å and $c = 33.1$ Å. Mercury derivatives were produced by soaking crystals in buffered stabilizing solutions containing 1 mM mercury acetate for 12 hours. The selenium derivative was obtained by incorporation of selenomethionine into the protein. A medium-resolution native data set (native 1) and a derivative data set (mercury 1) were collected at room temperature on a twin San Diego multiwire systems (SDMS) area detector with a Rigaku RU-200 rotating anode x-ray source. The Xuong-Hamlin method of data collection was used, and the images were processed and merged with SDMS software (*59*). A high-resolution native data set (native 2) and further derivative data sets (mercury 2 and selenium) were collected at room temperature on a MAR image plate detector on station 9.5 at the SRS Daresbury Laboratory (DRAL). The native 2 data set and those for the mercury 2 and selenium derivatives were processed with MOSFLM (*60*) and scaled with ROTAVATA and AGROVATA (*54*). The combination of the derivatives gave an overall figure of merit of 0.51 (acentric, 0.49; centric, 0.72). Model statistics were as follows: R_{cryst}, 0.209; rms bonds, 0.016 Å; and rms angles, 1.9°.

Data set (crystal and origin)	Data statistics					MIR statistics				
	Resolution (Å)	Reflections		R_{merge}*	Completeness (%)	Isomorphous difference (%)†	R_{Cullis}‡		Phasing power§	
		Total	Unique				Acentric	Centric	Acentric	Centric
Native 1: SDMS	2.3	29,152	10,786	0.073	91	N/A	N/A	N/A	N/A	N/A
Native 2: DRAL	1.9	40,402	16,391	0.029	89	N/A	N/A	N/A	N/A	N/A
Mercury 1: SDMS	2.3	11,318	9,116	0.111	77	30.0	0.80	0.66	0.93	1.02
Mercury 2: DRAL	2.5	17,515	7,197	0.045	88	24.0	0.85	0.75	1.00	0.85
Selenium: DRAL	2.5	15,760	7,111	0.057	87	13.0	0.86	0.56	1.65	1.47

*$R_{merge} = \Sigma_{hkl}|I_i - I_m|/\Sigma_{hkl}I_m$, where I_i and I_m are the observed intensity and mean intensity of related reflections, respectively. †Isomorphous difference $= \Sigma||F_{PH}| - |F_P||/\Sigma|F_P|$, where F_{PH} and F_P are the structure factor amplitudes for derivative and native crystals, respectively. ‡R_{Cullis} = (lack of closure)/(isomorphous difference). §Phasing power = F_H/lack of closure, where F_H is the calculated value for the structure factor due to a heavy atom in a derivative.

the normally allowed regions, and examination of Chi1-Chi2 plots for all residue types showed no side chains in unfavorable conformations. The average *B* value for all atoms of the complete monomer was 49.0 Å^2 (45.0 Å^2 for main chain atoms), but an examination of the *B*-factor distribution in the model showed a clear trend for higher *B* factors in the COOH-terminal half of the protein. The average *B* value for the NH_2-terminal segment (residues Met^1 to Glu^{106}) was 32.1 Å^2 (25.0 Å^2 for main chain atoms) and for the COOH-terminal segment (residues Val^{107} to Leu^{203}) was 73.6 Å^2 (71.0 Å^2 for main chain atoms). The latter segment includes seven residues with average *B* values ≥ 100.0 Å^2 but for which electron density is clearly observed in numerous omit maps.

The RuvA monomer has an overall L shape and is composed of three distinct domains and a flexible linker (Fig. 2C). Domain I comprises an NH_2-terminal six-stranded antiparallel β barrel (residues Met^1 to Asn^{64}; strands β1 to β6) with a single, short α helix (α1) intervening between β4 and β5. The central domain (domain II) contains five α helices (residues Asn^{65} to Pro^{142}; helices α2 to α6), and a flexible linker region (residues 143 to 155) connects it to domain III, which is composed of three α helices (residues Thr^{156} to Leu^{203}; helices α7 to α9). The strands in the β barrel in domain I form a classic Greek key motif. The barrel contacts domain II through hydrophobic interactions between residues in strands β4, β5, and β6 and helices α2 and α3, supplemented by a limited number of hydrogen bonds between main chain and side chain atoms in the two domains.

Although the chain trace within each of the three domains and between domains I and II is clear, the electron density map gave no indication of the position of the 13 residues that link domains II and III. Examination of the structure shows that only the connection of domains II and III from separate lobes of the tetramer is readily possible (Fig. 2D). A consequence of this connection is that there are no contacts between domain III and either domain I or II within a single subunit in the tetramer.

Gel filtration experiments on RuvA have shown it to be a tetramer in vitro (*27*). The crystal structure confirms this observation and further reveals it to have a somewhat unusual quaternary structure comprising fourfold rotational symmetry rather than the 222 symmetry usually found in tetrameric proteins. An obvious packing of monomers can be seen in the crystal lattice to form a tetramer with approximate dimensions of 80 Å by 80 Å by 45 Å. The four lobes of RuvA give rise to an overall shape reminiscent of a four-petaled flower, with convex and concave surfaces normal to the fourfold axis (Fig. 2, D and E). Grooves between the four lobes can be seen in the concave face radiating from a central pin formed by the four symmetry-related β turns between strands β5 and β6, which extend from the main body of the NH_2-terminal β barrel. The solvent-accessible area buried per monomer on formation of the tetramer was calculated with the program AREAIMOL (probe radius of 1.4 Å) (*31*) to be about 2500 Å^2 (assuming the flexible linker does not participate in the interface).

The subunit interface in the RuvA tetramer is formed by two distinct patches, one that arises mainly from interactions between residues in adjacent β barrels in domain I at the core of the tetramer and a second formed by residues in the helical bundle in domain III and residues from domains I and II of an adjacent monomer. The interaction between the β barrels consists primarily of the formation of a two-stranded β ribbon between the first six residues at the NH_2-terminus and residues in strand β4* (where the asterisk denotes residues in an adjacent monomer) plus a large hydrophobic contribution from contacts between residues in strands β1, β3, β5, β4*, β5*, and β6*. There are additional contacts between the NH_2-terminal Met residue and residues in strand β6*, plus a small number of ion pair interactions between

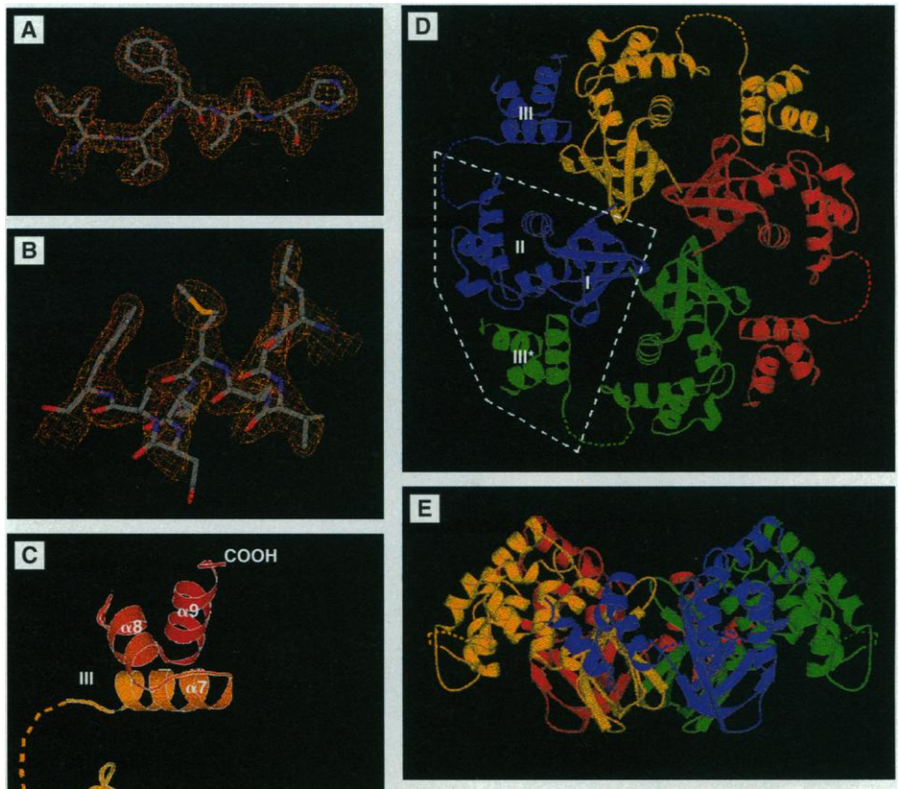

Fig. 2. Representations of the structure of RuvA. (**A**) Representative portion of strand β5 in the NH_2-terminal segment of the protein from a $|2F_O - F_C|$ map calculated at 1.9 Å resolution with the RuvA model in the later stages of refinement. (**B**) As in (A) but from helix α6 in the COOH-terminal segment of the protein. (**C**) A single subunit of the RuvA tetramer. The α helices (coils) and β strands (arrows) are numbered as in the text, and domains I, II, and III are indicated. The subunit is colored from blue through yellow to red from the NH_2 terminus to the COOH-terminus, and the flexible linker region is depicted as a dashed yellow line. (**D** and **E**) RuvA tetramer illustrating its fourfold symmetry and overall shape. The individual monomers are shown in red, blue, green, and orange-yellow, and the flexible linker regions are indicated by dashed lines. In (D) is shown a view along the fourfold symmetry axis into the concave face of the tetramer. An individual "lobe" is delineated by a white dashed line, and the subunit domains are labeled as in the text. In (E) is shown a view perpendicular to the fourfold symmetry axis along a groove in the concave surface [produced with BOBSCRIPT (R. Esnouf, personal communication), a modified version of MOLSCRIPT (*56*)].

glutamate residues in strands β2, β3, and β4 and Arg and Lys residues in strand β1* and helix α2*. The intimate contacts made by the β barrels of domain I leave only a small solvent channel down the fourfold axis that is about 2 Å wide at its narrowest point where the symmetry-related side chains of Gln^{58} approach each other. The interface formed by contact of residues from the helical bundle in domain III with the neighboring monomer is purely hydrophobic and involves residues in helices α7 and α9 and those in the short helix α1*, the COOH-terminal end of helix α3*, the loop between helices α5* and α6*, and the turn between strands β2* and β3*. There is a solvent channel between the lobes of the tetramer that extends from the convex to the concave surface and is about 5 Å wide at its narrowest point between the main chain (around His^{136}) and the side chain of Gln^{13}*.

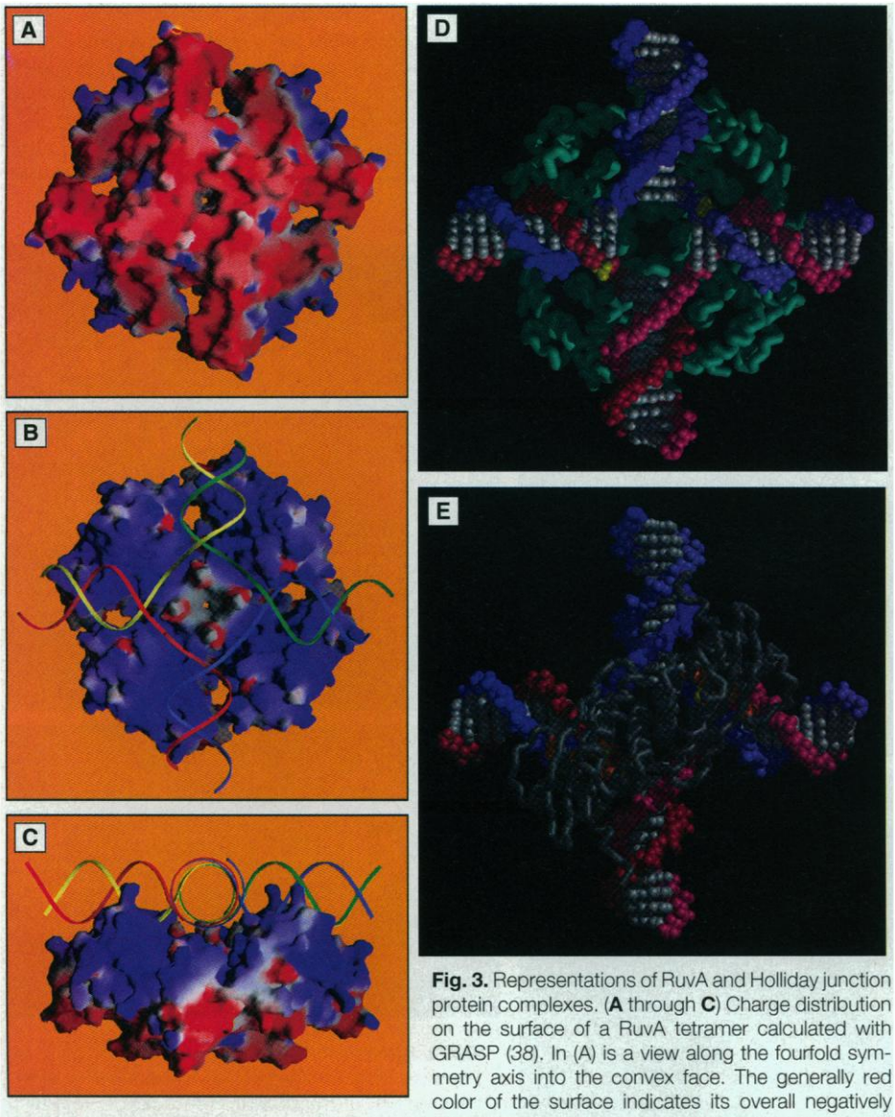

Fig. 3. Representations of RuvA and Holliday junction protein complexes. (**A** through **C**) Charge distribution on the surface of a RuvA tetramer calculated with GRASP (*38*). In (A) is a view along the fourfold symmetry axis into the convex face. The generally red color of the surface indicates its overall negatively charged nature. In (B) is shown a view along the fourfold symmetry axis into the mainly blue concave face, which has an overall positive charge. Note, however, the small red region around the central pin, indicative of a patch of negatively charged surface potential. Also shown is a model for the binding of a Holliday junction by RuvA. The DNA is shown with its phosphate backbones as continuous ribbons colored red, blue, green and yellow. In (C) is shown a view of the RuvA–Holliday junction complex perpendicular to the fourfold axis along a groove in the concave surface of RuvA. (**D** and **E**) Models for the interaction of RuvA and RuvC with a square planar Holliday junction model. The proteins are shown as α-carbon backbone traces. The DNA is shown in an all-atom representation, and the backbones of individual strands are blue, light blue, red, and pink. The phosphate groups of one of the two possible pairs of RuvC cleavage sites are yellow. In (D) is shown the RuvA tetramer with its subunits colored cyan. In (E) is shown the RuvC dimer [PDB entry 1HJR (*45*)] with its subunits colored gray. Residues Asp^{7}, Glu^{66}, Asp^{138}, and Asp^{141} from each monomer, which have been proposed by mutational analysis to be catalytically important (*45*), are shown in an all-atom representation and are colored orange. The models in (D) and (E) were produced with the program MIDAS (*57*). An animated model of the migration of the RuvA-junction complex is available on the Internet (*58*).

The program PROTEP (*32*) was used to compare the three-dimensional coordinates of RuvA with those of all other proteins in the April 1996 release of the Brookhaven Protein Data Bank (*33*). Notable similarities were found between the NH_2-terminal domain I of RuvA and the nucleic acid–binding proteins staphylococcal nuclease, the anticodon-binding domain of Asp tRNA synthetase, and the major cold-shock protein from *Bacillus subtilis* (*34*). The PROTEP search showed a similarity among RuvA domain III, three α helices from the fingers domain of DNA polymerase β (*35*), and helices α2, α3, and α4 in domain II of RuvA itself. Most interestingly, α2, α3, α5, and α6, four of the five α helices forming domain II, overlapped well with the catalytic region of the fingers domain of DNA polymerase β (*35*) and with the fingers domain of the Klenow fragment of DNA polymerase I (*36*). Additionally, we note that RuvA possesses two copies of a secondary structural motif termed a helix-hairpin-helix as proposed by sequence comparison studies (*37*).

The sequences of several RuvA-like proteins have been determined. When the positions of conserved residues are highlighted on the three-dimensional structure of *E. coli* RuvA, there is a marked preponderance of such residues in the core of the protein, stabilizing the intra- and intersubunit contacts, and on the concave surface of the tetramer. We analyzed the distribution of charge on the protein surface by computing the electrostatic surface potential of the RuvA tetramer with the program GRASP (*38*). This analysis revealed a striking difference in the charge distribution over the surface of the tetramer; the nonconserved convex surface of the tetramer was notably negatively charged, and the highly conserved concave surface was predominantly positively charged, particularly along the grooves between the lobes (Fig. 3). However, analysis of the surface potential of the concave surface also showed a small negatively charged region, formed around the fourfold axis by the central pin, that arises from the side chains of the conserved residues Glu^{55} and Asp^{56}. The electrostatic surface potential of B-form DNA (B-DNA) is dominated by the negative charge on the phosphate backbone, and thus it might be expected to interact favorably with regions of positive electrostatic potential and unfavorably with those of negative electrostatic potential. The distribution of charge on the

tetramer and the observed sequence conservation together provide strong support for the view that the concave surface of RuvA provides the site for DNA binding.

In an attempt to understand the mode of binding of RuvA to DNA and the possible functional implications of such binding, we constructed a simple model of a Holliday junction from four 12–base pair (bp) sections of double-stranded B-DNA whose helical axes were coplanar, coincident, and related by a fourfold axis normal to this plane (*39*). A feature of this model is the presence of a hole of about 17 Å in diameter at the central fourfold axis of the junction. In our model, the two faces of the junction are distinct with either the major or minor groove of the DNA located centrally in each arm. There are no unpaired bases in the DNA model and unstacking of bases occurs only at the central crossover point of the junction. However, there is necessarily a transient unpairing of bases during branch migration because the bases translocate from parent to daughter duplexes. This square planar arrangement of the arms of the DNA in the Holliday junction is consistent with the model proposed by West and colleagues from analysis of electron microscopy images and gel retardation studies on complexes of RuvA with Holliday junctions (*14*).

The model of the junction was then manually docked onto the concave surface of the RuvA tetramer, maintaining colinearity of the fourfold axes of the junction and the tetramer. Thus, the only parameters that can be varied are the relative rotation about the common fourfold axis, the separation of the DNA and protein, and the face of the junction docked to the protein. It was immediately apparent that with this arrangement, the central hole between the arms of the junction is located above the central negatively charged pin on the concave surface. A good fit of the DNA onto the protein as judged by complementarity of their surface shapes and charges was observed when the axes of the DNA helical arms lay along the grooves in the concave surface of the protein with about 8 bp of each helical arm in contact with protein (Fig. 3B). In the model, the pairs of parent and daughter duplexes are on opposite sides of the central pin. The negatively charged phosphate backbone of the DNA is positioned on the surface of the protein along the grooves in the concave face and thus close to the regions of highest positive charge potential (Fig. 3C). However, there are gaps between the lobes of the tetramer and it is therefore conceivable that there may be conformational changes on binding either DNA or RuvB that could modify the shape of the RuvA tetramer and allow the development of more intimate contact between the Holliday junction DNA and RuvA.

The face of the DNA docked to the protein in our model was selected so that the major groove in the B-form DNA was adjacent to the protein surface and not accessible to deoxyribonuclease I activity, consistent with the results of footprinting experiments involving RuvA and synthetic Holliday junctions (*40*) and also with a simple model for resolution of the junction by RuvC (see below). However, on the basis of the model alone we cannot rule out the possibility that the complex is formed with the minor groove facing RuvA because reasonable contacts can also be formed by flexible Arg and Lys side chains with the DNA in this orientation. In either orientation, the model allows ready translocation of the unpaired DNA bases over the protein surface between the duplex arms as they feed through the crossover point during branch migration of the junction.

Our model assumes a tetrameric assembly of RuvA and junction DNA, although it is possible to construct a model in which two tetramers of RuvA sandwich a junction by binding to opposite faces of the DNA. Gel electrophoretic analysis shows that RuvA forms two well-defined complexes with junction DNA, one of which migrates much more slowly than the other (*10*). An octameric assembly could account for the slower migrating species. Whether such an assembly would be biologically relevant is another matter. Sandwiching the junction would prevent access by other proteins and exclude the idea that RuvC resolves junctions in a complex with RuvAB (see below). The available evidence is inconclusive. In vivo, RuvA certainly interferes with the ability of the RusA resolvase to replace RuvC (*24*), and its overproduction relative to RuvB is detrimental to repair (*41*). In vitro RuvA inhibits branch migration by RecG (*24*) and resolution by both RuvC and RusA (*42*). Nevertheless, the fact remains that whereas the RusA resolvase can work efficiently in vivo without RuvAB, RuvC cannot (*23*, *24*).

Previous studies showed that Holliday junctions adopt a stacked-X structure in the presence of divalent cations (*43*). This configuration presents a steric barrier that hinders spontaneous branch migration in vitro (*44*). RuvAB drives branch migration efficiently (*11*) and is thought to overcome the steric barrier by holding the junction in a square planar configuration (*14*). The structure of RuvA reveals how this might be achieved and provides insights into the molecular mechanism of the branch migration reaction. The RuvB hexamer rings assembled on homologous duplex DNA arms flanking the RuvA junction complex (Fig. 1B) provide the motor for the relative motion of the DNA across the surface of the RuvA tetramer by using energy from the hydrolysis of adenosine triphosphate (ATP). The central pin on the RuvA concave surface is positioned such that the two strands of the incoming duplex DNA are encouraged to separate as a result of the repulsive interaction between the negative charges of the side chains that decorate the central pin and the phosphate backbones of the two strands. However, the lack of a strictly equivalent, negatively charged pin motif in the sequence of a RuvA-like protein from *Mycobacterium genitalium* might suggest that a steric mechanism also operates to separate the strands. The separated strands of the parent duplex are then channeled between the central pin and the symmetry-related loops between helices α2 and α3 into the orthogonal grooves in the protein surface where they anneal with base pairs from the other incoming parent DNA duplex to form the outgoing daughter duplexes (Fig. 3, B and C). A feature of our model is that only a single base pair from each of the parent duplexes needs to be separated at any given instant during translocation before the component bases subsequently reanneal with new partners to form the daughter duplexes. During the translocation process, the fourfold symmetry of the static RuvA junction complex (Fig. 3D) is reduced to twofold symmetry such as is observed in the structure of RuvC (*45*) and as shown in the complex model (Fig. 3E). As modeled here, for each base pair that migrates through the junction, the DNA must be rotated by 36° and translated by 3.4 Å. This rotation, which is also a feature of the model proposed by Parsons *et al.* (*14*), requires a change in the supercoiling of both parent and daughter strands, which might be relaxed by the action of topoisomerases.

The chosen DNA orientation in our model results in the scissile bonds that are cleaved by the action of the RuvC resolvase being exposed to the solvent and hence readily accessible to the enzyme. The structure of RuvC has been determined (*45*), and the protein has been shown to be a dimer whose two active sites are separated by about 30 Å. This separation is in excellent agreement with the distance of about 28 Å between the scissile bonds in our model of the Holliday junction (Fig. 3, D and E). However, when the RuvC dimer is docked to this DNA model, there is some steric conflict between a pair of twofold related loops in the RuvC dimer (residues Val^{68} to Lys^{72}) and the DNA backbone as noted by Ariyoshi *et al.* (*46*). An alternative model was proposed for the configuration of the DNA (*46*), but it was noted that these

loops are flexible. Thus, these loops may be susceptible to conformational change upon RuvC binding to its DNA target. However, perhaps RuvC does take the junction from its complex with RuvA and folds it into an alternative configuration as part of the cleavage reaction. This would be consistent with the recent analysis of RuvC-junction complexes (*18*).

RuvC resolves Holliday junctions in either of two possible orientations to give either noncrossover (patch) or crossover (splice) products (Fig. 1) (*2*, *16*). The RuvAB–junction assembly envisaged here could accommodate a dimer of RuvC bound to the opposite face of the junction DNA from RuvA and between RuvB rings located on opposing arms of the complex. If no specific contacts are formed between RuvB and RuvC, the orientation of cleavage would be arbitrary and equal proportions of patch and splice products might be expected, regardless of which pair of duplex arms is bound by RuvB. However, the formation of specific contacts would orient the binding of RuvC to the junction, and this would determine which pair of bonds was cleaved by RuvC and the resulting nature of the products of resolution. Thus, the pair of arms bound by RuvB and the factors affecting this binding would be critical in deciding the fate of the junction by influencing the choice of orientation of RuvC. There is no direct evidence that RuvC cleaves junctions in a complex with RuvAB. However, genetic observations (*23*, *24*) are consistent with this view and the complementarity between the structure of RuvC and the RuvA–Holliday junction model proposed here makes it a tantalizing possibility.

Branch migration is a specialized form of DNA helicase activity in which complementary strands from two homologous duplexes are unwound and then rewound to form hybrid duplexes. The structure of RuvA described here and our modeling of a RuvA-junction DNA complex provide the first detailed insights into the reaction mechanism. They suggest how, in a RuvAB complex, ATP hydrolysis by RuvB rotates DNA across the surface of the RuvA tetramer, which is exquisitely carved to open the junction point, split apart the strands of the incoming helices, and channel them into new helices that move out of the RuvAB structure.

Although RuvAB is clearly designed to act on a four-way junction in DNA it will also unwind a three-way junction and related structures with reasonable efficiency (*12*, *46*). It is easy to envisage how a three-way junction could be accommodated around the central pin on the RuvA surface and how a RuvB ring assembled on one duplex arm could lead to the observed unwinding of one strand. The same principle could be applied to other DNA (or RNA) structures. A RuvA-like pin coupled to a suitable protein domain for structure-specific binding and an appropriate motor could prove to be a general mechanism for strand separation applicable to many helicases.

Holliday junctions are universal intermediates in genetic recombination. Homologs of RecA protein, which generates these intermediates, have been discovered in many eukaryotes (*5*, *47*), whereas RuvC-like resolvases have been found in yeast and mammalian cells (*6*). Mutations in homologs of RecQ helicase are responsible for human genetic diseases associated with defective repair, aberrant recombination, and aging (*48*). Hexameric ring helicases such as RuvB are common components of protein machines assembled at replication forks, where they help to drive strand separation and prime DNA synthesis. The striking similarity between RuvB protein and the phage T7 gp4 and SV40 large T antigen replicative helicases suggests that the ring structure arose early in evolution and is widely conserved (*49*). Thus, it is tempting to speculate that the RuvA mechanism of strand separation and the RuvABC system for processing Holliday junctions may be a general paradigm, not only for specific repair processes in bacteria but also for other processes of genetic recombination, both in prokaryotes and in higher organisms. Recombination is a fundamental process that is involved in DNA repair, chromsosomal segregation during cell division, and generation of genetic diversity. A structural insight into the RuvA-Holliday junction system may therefore prove to be a valuable step in our understanding of these widespread and crucial biological processes.

REFERENCES AND NOTES

1. R. Holliday, *Genet. Res.* **5**, 282 (1964).
2. F. Stahl, *Genetics* **138**, 241 (1994).
3. R. G. Lloyd and K. B. Low, in Escherichia coli and Salmonella typhimurium *Cellular and Molecular Biology*, F. C. Neidhardt *et al.*, Eds. (American Society for Microbiology, Washington, DC, ed. 2, in press).
4. T. Ogawa, X. Yu, A. Shinohara, E. H. Egelman, *Science* **259**, 1896 (1993).
5. A. Shinohara *et al.*, *Nature Genet.* **4**, 239 (1993).
6. M. F. White and D. M. J. Lilley, *J. Mol. Biol.* **257**, 330 (1996); H. Hyde, A. Davies, F. Benson, S. West, *J. Biol. Chem.* **269**, 5202 (1994).
7. S. C. Kowalczykowski, D. A. Dixon, A. K. Eggleston, S. D. Lauder, W. M. Rehrauer, *Microbiol. Rev.* **58**, 401 (1994); S. C. West, *Annu. Rev. Biochem.* **61**, 603 (1992).
8. S. C. West, *J. Bacteriol.* **178**, 1237 (1996).
9. H. Iwasaki, M. Takahagi, A. Nakata, H. Shinagawa, *Genes Dev.* **6**, 2214 (1992).
10. C. A. Parsons, I. Tsaneva, R. G. Lloyd, S. C. West, *Proc. Natl. Acad. Sci. U.S.A.* **89**, 5452 (1992).
11. I. R. Tsaneva, B. Müller, S. C. West, *Cell* **69**, 1171 (1992).
12. ———, *Proc. Natl. Acad. Sci. U.S.A.* **90**, 1315 (1993); I. R. Tsaneva and S. C. West, *J. Biol. Chem.* **269**, 26552 (1994).
13. A. Stasiak *et al.*, *Proc. Natl. Acad. Sci. U.S.A.* **91**, 7618 (1994).
14. C. A. Parsons, A. Stasiak, R. J. Bennett, S. C. West, *Nature* **374**, 375 (1995).
15. B. Connolly *et al.*, *Proc. Natl. Acad. Sci. U.S.A.* **88**, 6063 (1991); H. Iwasaki, M. Takahagi, T. Shiba, A. Nakata, H. Shinagawa, *EMBO J.* **10**, 4381 (1991).
16. H. J. Dunderdale *et al.*, *Nature* **354**, 506 (1991).
17. H. J. Dunderdale, G. J. Sharples, R. G. Lloyd, S. C. West, *J. Biol. Chem.* **269**, 5187 (1994).
18. R. J. Bennett and S. C. West, *J. Mol. Biol.* **252**, 213 (1995).
19. D. R. Duckett *et al.*, *Cell* **55**, 79 (1988).
20. R. Shah, R. J. Bennett, S. C. West, *ibid.* **79**, 853 (1994).
21. R. J. Bennett and S. C. West, *Proc. Natl. Acad. Sci. U.S.A.* **92**, 5635 (1995).
22. R. G. Lloyd and G. J. Sharples, *EMBO J.* **12**, 17 (1993); M. C. Whitby, S. Vincent, R. G. Lloyd, *ibid.* **13**, 5220 (1994); G. J. Sharples, S. C. Chan, A. A. Mahdi, M. C. Whitby, R. G. Lloyd, *ibid.*, p. 6133.
23. A. A. Mahdi, G. J. Sharples, T. N. Mandal, R. G. Lloyd, *J. Mol. Biol.* **257**, 561 (1996).
24. T. N. Mandal, A. A. Mahdi, G. J. Sharples, R. G. Lloyd, *J. Bacteriol.* **175**, 4325 (1993).
25. S. E. Sedelnikova *et al.*, *Acta Crystallogr. D*, in press.
26. A. H. Mitchell and S. C. West, *J. Mol. Biol.* **243**, 208 (1994).
27. I. R. Tsaneva, G. T. Illing, R. G. Lloyd, S. C. West, *Mol. Gen. Genet.* **235**, 1 (1992).
28. Phases were calculated and refined from the two derivative data sets (Table 1) with the program MLPHARE (*50*). A preliminary 2.5 Å MIR map was calculated and inspection revealed the molecular boundary of the tetramer to be a four-lobed structure. A trace linking the local regions of highest electron density in the map was made with the BONES program from the O suite of programs (*51*). This trace enabled the placement of "dummy" residues that best matched the observed density using the FRODO program (*52*) on an Evans and Sutherland ESV workstation. A new map was calculated by combining the phase information from this partial structure with that from MIR. Through iteration of this dummy residue approach, the map was steadily improved and eventually specific residues could be identified and the sequence aligned to the density. The sequence alignment was greatly helped by the location of the selenomethionine residues, which acted as markers in the electron density map. When the positions of about 75% of the residues had been determined, of which two-thirds had sequences assigned, the model was submitted to least squares refinement with the program TNT (*53*), which also incorporated a correction for the solvent continuum. The initial R factor was from 0.44 to 2.5 Å resolution. Phases calculated from this refined model with the program SFALL (*54*) were then combined with the MIR phases through use of the program SIGMAA (*54*). A $|2F_O - F_C|\alpha_{comb}$ map was produced, where α_{comb} is the appropriately weighted combination of MIR and the calculated phase, and more residues were identified and fitted. Further rounds of model building and refinement were carried out and during this process the resolution was gradually extended to 1.9 Å with data collected at the SRS Daresbury laboratory. In later stages, a low-resolution cutoff was applied at 15 Å and a total of 54 solvent molecules assigned. Omit maps were calculated for the regions of the model where the density was poor and refined B factors were high. An R factor of 20.9% was obtained for all data (no σ cutoff) in the resolution range from 15 to 1.9 Å.
29. The strain used was *E. coli* AM103, a BL21(DE3) *met*$^-$ derivative transformed with the *ruvA*$^+$ construct pAM159 (*25*).
30. A procedure for searching difference Patterson maps for the sites of heavy atoms with a genetic algorithm technique has been developed (T. J. Palmer and P. J. Artymiuk unpublished data).
31. B. Lee and F. M. Richards, *J. Mol. Biol.* **55**, 379 (1971).
32. H. M. Grindley, P. J. Artymiuk, D. W. Rice, P. Willett, *ibid.* **229**, 707 (1993).

33. F. C. Bernstein *et al.*, *ibid.* **12**, 535 (1977).
34. P. J. Loll and E. E. Lattman, *Proteins Struct. Funct. Genet.* **5**, 183 (1989); M. Ruff *et al.*, *Science* **252**, 1682 (1991); H. Schindelin, M. A. Marahiel, U. Heinemann, *Nature* **364**, 164 (1993).
35. H. Pelletier, M. R. Sawaya, A. Kumar, S. H. Wilson, J. Kraut, *Science* **264**, 1891 (1994); J. F. Davies, R. J. Almassy, Z. Hostomska, R. A. Ferre, Z. Hostomsky, *Cell* **76**, 1123 (1994).
36. L. S. Beese, V. Derbyshire, T. A. Steitz, *Science* **260**, 352 (1993).
37. M. M. Thayer, H. Ahern, D. Xing, R. P. Cunningham, J. A. Tainer, *EMBO J.* **14**, 4108 (1995); A. J. Doherty, L. C. Serpell, C. P. Ponting, *Nucleic Acids Res.* **24**, 2488 (1996).
38. A. Nicholls, K. A. Sharp, B. Honig, *Proteins* **11**, 281 (1991). The protein surface in Fig. 3, A through C, is colored according to the calculated electrostatic potential due to full charges on the protein; red when it is less than $\div 5.0$ kcal(mol · e)$^{-1}$ and blue when it exceeds 5.0 kcal(mol · e)$^{-1}$, where *e* is the unit charge.
39. The DNA model proved straightforward to construct by making simple rotations and translations of the helical axes that enabled the 5′ to 3′ and 3′ to 5′ phosphate backbone strands of each duplex section to be joined to those of adjacent sections. The covalent bond distances and angles are those of standard B-DNA (*55*), except for the ε and ζ torsion angles adopted by the single linking phosphate group at the 90° bend in each chain, which have values of 276° and 222°, respectively. These torsion angles are stereochemically reasonable and compare with values for ε of 170° and for ζ of 257° in straight standard B-DNA (*55*).
40. K. Hiom and S. C. West, *Cell* **80**, 787 (1995).
41. G. J. Sharples, F. E. Benson, G. T. Illing, R. G. Lloyd, *Mol. Gen. Genet.* **221**, 219 (1990).
42. M. C. Whitby, S. N. Chan, R. G. Lloyd, unpublished data.
43. D. R. Duckett, A. I. H. Murchie, D. M. J. Lilley, *EMBO J.* **9**, 583 (1990).
44. I. G. Panyutin and P. Hsieh, *Proc. Natl. Acad. Sci. U.S.A.* **91**, 2021 (1994); I. G. Panyutin, I. Biswas, P. Hsieh, *EMBO J.* **14**, 1819 (1995).
45. M. Ariyoshi *et al.*, *Cell* **78**, 1063 (1994).
46. R. G. Lloyd and G. J. Sharples, *Nucleic Acids Res.* **21**, 1719 (1993).
47. P. Sung and D. L. Robberson, *Cell* **82**, 453 (1995); K. Maeshima, K. Morimatsu, A. Shinohara, T. Horii, *Gene* **160**, 195 (1995).
48. C.-E. Yu *et al.*, *Science* **272**, 258 (1996); N. A. Ellis *et al.*, *Cell* **83**, 655 (1995).
49. E. H. Egelman, X. Yu, R. Wild, M. M. Hingorani, S. S. Patel, *Proc. Natl. Acad. Sci. U.S.A.* **92**, 3869 (1995).
50. Z. Otwinowski, in *Proceedings of the CCP4 Study Weekend*, W. Wolf, P. R. Evans, A. G. W. Leslie, Eds. (SERC Daresbury Laboratory, Warrington, UK, 1991), p. 80.
51. T. A. Jones, J. Y. Zou, S. W. Cowan, M. Kjeldgaard, *Acta Crystallogr. A* **47**, 110 (1991).
52. T. A. Jones, *J. Appl. Crystallogr.* **11**, 268 (1978).
53. D. E. Tronrud, L. F. Ten Eyck, B. W. Matthews, *Acta Crystallogr. A* **43**, 489 (1987).
54. Collaborative Computing Project no. 4, *Acta Crystallogr. D* **50**, 760 (1994).
55. S. Arnott, S. D. Dover, A. J. Wonacott, *Acta Crystallogr. B* **25**, 2192 (1969).
56. P. J. Kraulis, *J. Appl. Crystallogr.* **24**, 946 (1991).
57. T. E. Ferrin, C. C. Huang, L. E. Jarvis, R. Langridge, *J. Mol. Graphics* **6**, 13 (1988).
58. The animated model as proposed in this paper is available on the Web (in the United Kingdom) at http://www.shef.ac.uk/~mbb/ruva.html and (in the United States) at http://www.sdsc.edu/journals/mbb/ruva.html.
59. R. Hamlin, *Methods Enzymol.* **114**, 416 (1985); N. H. Xuong, C. Nielsen, R. Hamlin, D. Anderson, *J. Appl. Crystallogr.* **18**, 324 (1985); A. J. Howard, C. Nielsen, N. H. Xuong, *Methods Enzymol.* **114**, 452 (1985).
60. A. G. W. Leslie, in *Joint CCP4 and ESF-EACBM Newsletter on Protein Crystallography 26*, (SERC Daresbury Laboratory, Warrington, UK, 1992).

61. We thank M. Legg (Zeneca Agrochemicals, Jealott's Hill, UK) for fermentation of the recombinant cells incorporating selenomethionine; the support staff at the Synchrotron Radiation Source, Daresbury Laboratory, Warrington, UK, for assistance with station alignment; and T. J. Palmer for the program used to analyze the selenomethionine Patterson map. Supported by grants from the UK Biotechnology and Biological Sciences Research Council (BBSRC) and the UK Medical Research Council to P.J.A., R.G.L., and D.W.R., and the Wellcome Trust to P.J.A. and D.W.R. J.B.R. is a BBSRC Technology Foresight Junior Research Fellow. G.J.S. is a Royal Society University Research Fellow. The Krebs Institute is a designated BBSRC Biomolecular Science Centre.

17 May 1996; accepted 2 August 1996

Resistance to *Leishmania major* Induced by Tolerance to a Single Antigen

Valérie Julia, Minoo Rassoulzadegan, Nicolas Glaichenhaus*

In mice, susceptibility to *Leishmania major* is associated with the early expansion of T helper 2 cells (T_H2) cells, but nothing is known of the specificity of these cells. A previously identified antigen, *Leishmania* homolog of receptors for activated C kinase (LACK), was found to be the focus of this initial response. Mice made tolerant to LACK by the transgenic expression of the antigen in the thymus exhibited both a diminished T_H2 response and a healing phenotype. Thus, T cells that are activated early and are reactive to a single antigen play a pivotal role in directing the immune response to the entire parasite.

The outcome of an infection can be determined by the balance between interferon-γ (IFN-γ)–secreting (T_H1) and interleukin-4 (IL-4)–secreting (T_H2) cells (*1*). In experimental murine leishmaniasis, susceptible mice such as those of the BALB/c strain respond to infection with the preferential expansion of IL-4–producing T_H2 cells (*2*). Neutralization of IL-4 within the first week of infection prevents the emergence of the T_H2 response and allows the generation of potentially protective T_H1 cells and the development of a healing phenotype (*3*). IL-4 appears to be both the main inducer of T_H2 responses and an inhibitor of T_H1 responses (*4*). An early burst of IL-4 production is detected in the lymph nodes of infected mice, with $CD4^+$ T cells being the main cellular source (*5*). It has been proposed that these early-activated IL-4–secreting cells belong to the recently described subpopulation of natural killer (NK) T cells that react to the nonclassical major histocompatibility complex (MHC) class I protein CD1 (*6*), but recent experiments using β_2-microglobulin–deficient mice, in which NK T cells are not positively selected, do not support this hypothesis (*7*). Alternatively, these IL-4–secreting $CD4^+$ T cells may be parasite-specific cells that are activated very rapidly after infection. The work described here is aimed at identifying the parasite antigens that trigger this early burst of IL-4 and at down-regulating this response by means of antigen-specific tolerogenic approaches.

We recently described the expression cloning of a 36-kD *Leishmania* antigen, LACK (*8*). Most LACK-reactive T cells used the same $V_\alpha8$ and $V_\beta4$ variable T cell receptor regions and reacted to the same antigenic determinant (amino acids 158 through 173). Expansion of $V_\alpha8^+V_\beta4^+$ $CD4^+$ T cells occurred in the lymph nodes of infected mice (*9*), which suggests that LACK was the focus of the initial immune response against the parasite (*8*). To test this, we generated a panel of 30 parasite-specific short-term T cell clones from the lymph nodes of infected BALB/c mice (*10*). Ten of these clones responded to LACK; all secreted IL-4 but not IFN-γ, which suggests that LACK was a preferential target of the early anti-parasite immune response and that early-activated LACK-reactive T cells exhibited a T_H2 phenotype. This was confirmed by monitoring of the number and the phenotype of LACK-reactive T cells by means of an antigen-specific ELISPOT assay (Fig. 1). Six days after infection, lymph node $CD4^+$ T cells were prepared and incubated with syngeneic antigen-presenting cells (APCs) with or without an optimal concentration of LACK peptide or soluble extracts from the parasite soluble *Leishmania* antigens (SLA)] (*11*). Infection induced a strong response against LACK, and most of the early-activated T cells secreted IL-4 or IL-5 or both (Fig. 1). This contrasts with the exclusively T_H1 response directed to the main antigenic determinant of the major promastigote surface protease, GP63 (*12*), whereas responses to other parasite determinants, including the recently identified LDP23 antigen (*13*), were of lesser magnitude.

The early burst of LACK-induced T_H2-

V. Julia and N. Glaichenhaus, CNRS, Institut de Pharmacologie Moléculaire et Cellulaire, 660 Route des Lucioles, 06560 Valbonne, France.
M. Rassoulzadegan, Unité INSERM 273, Faculté des Sciences, 06108 Nice Cedex 2, France.

*To whom correspondence should be addressed. E-mail: GLAICHEN@naxos.unice.fr